A Case Study of the Collapse of Slender Pillars Affected by Through-Going Discontinuities at a Limestone Mine in Pennsylvania

Gabriel S. Esterhuizen[1], **Paul L. Tyrna**[2], **Michael M. Murphy**[1]

[1]NIOSH Pittsburgh Mining Research Division, 626 Cochran's Mill Road, Pittsburgh, PA, USA

[2]MSHA Technical Support Group, Triadelphia, VW, USA

Abstract

The sudden collapse of approximately 3 Ha of room-and-pillar workings at a limestone mine in southwestern Pennsylvania in 2015 resulted in an air blast that injured three mine workers. Subsequent investigations showed that an area encompassing 35 pillars had collapsed. The pillars were 9–10 m wide and up to 18 m high. A notable geologic feature is the through-going joints that dip at 50–80° and can extend from the roof to the floor of the pillars. These structures are thought to have weakened the pillars well below the strength that is predicted by empirical equations for hard-rock pillar design. This paper presents the relevant geotechnical data related to the collapsed area and numerical model results that were used to estimate the pillar loading underneath the variable topography, and compares the pillar loads to some established hard-rock pillar strength equations. The outcome is also compared to a strength equation that was developed specifically for limestone mines in which the negative impact of large angular discontinuities is explicitly accounted for. The results show that established hard-rock pillar strength equations do not adequately account for the impact of large through-going discontinuities on the strength of slender pillars. The equations would have significantly overestimated the strength of the pillars at the case study mine. The critical state of the workings would have been predicted correctly by the limestone pillar strength equation that accounts for the large discontinuities.

Keywords

Mining; Pillars; Pillar strength; Pillar collapse; Limestone; Discontinuities

1 Introduction

On April 29, 2015, three mine workers were waiting near the access portal of an underground limestone mine in southwestern Pennsylvania when they heard something that

✉Gabriel S. Esterhuizen, eee5@cdc.gov.

sounded like shots being fired in the mine. This was followed by a massive collapse of the room-and-pillar workings in the mine. The air blast from the collapse knocked the mine workers to the ground, causing serious injuries to each one. Subsequent investigations revealed that subsidence of the mountainside overlying the mine workings had occurred. The subsidence area encompassed about 3 Ha. Underground inspections to delineate the collapsed area showed that about 35 pillars had collapsed. A wide-angle, aerial camera view of the mine showing the access portal and the subsidence area is presented in Fig. 1. The mine owners have requested that the name of the mine operation remains anonymous in this publication and will be referred to as 'the case study mine'.

The objective of this paper is to describe the geotechnical and mining factors associated with the pillar failure and to demonstrate how large through-going discontinuities reduced the pillar strength well below the strength that would have been predicted by established hard-rock pillar strength equations. An equation that explicitly accounts for the impact of such large discontinuities is presented, and it is shown that this equation would have identified the critical stability of the pillars at the case study mine.

2 Geotechnical Parameters

2.1 Geologic Setting

The case study mine is located within the Appalachian Plateau province and is situated 120 m beneath the crest of Chestnut Ridge in southwestern Pennsylvania, USA. The Appalachian plateau is the westernmost physiographic province of the Appalachian mountain belt (Fig. 2) and is characterized by broad folding with dips ranging from 20° to less than 5° and wavelengths ranging from 8 to 32 km. Structural relief ranges from less than 100 m to more than 1000 m (Kerrigan 2016).

The Appalachian Plateau is bounded on the east by the Allegheny structural front, which marks the transition into the more intense structural deformation in the Valley and Ridge province (Rodgers 1970; Sak et al. 2012; Trapp and Horn 1997). Chestnut Ridge is a northeast trending, roughly 150 km long, doubly plunging anticline with a maximum topographical relief of 300 m in the vicinity of the mine. It is asymmetrical, with steeper dipping strata on the northwest side.

The Loyalhanna limestone extracted at the mine typically occurs at depth in the region, but is mined in numerous locations where folding has brought it nearer to the surface. The folding of the Loyalhanna limestone is gentle and is hardly noticeable at the scale of the collapsed mine workings. In southwestern Pennsylvania, the Loyalhanna is stratigraphically a lower member of the 1000- to 1500-m-thick, Mississippian-age Mauch Chunk Formation. The Loyalhanna limestone has a maximum thickness of 30 m, but is typically 20 m thick in the Chestnut Ridge mines. It is light to greenish gray and compositionally ranges from a calcareous sandstone to a sandy limestone (Edmunds et al. 1979). At the mine, the Loyalhanna limestone bed is overlain by distinctive reddish-brown mudstones, shales, and siltstones of the Mauch Chunk beds, as shown in Fig. 3.

2.2 Geologic Structure

Geologic structure typically associated with folding in the Appalachian plateau includes faults and joints. Transverse and longitudinal joints that strike perpendicular and parallel to fold axes, respectively, are typically dominant (Hatcher et al. 1989; Nickelsen and Hough 1967). In areas were salt deposits underlie deformed strata, shallow, low angle thrust faults, parallel to fold axes occur (Gillespie and Kampfer 2017). These faults have been interpreted as late-stage breakthrough faults (Mount 2014). All three of these types of geologic structure were observed at the study mine and are consistent with other structural patterns described in previous studies (Iannacchione and Coyle 2002).

A well-defined thrust fault was visible in the highwall immediately north of the Haulage (south) Portal. The N25°E striking fault was planar with approximately 1.5 m of apparent offset. Dip was calculated at 15° southeast. The fault intersected the top of the mining horizon near the south portal and intersected the surface along the southeast edge of the pillar collapse subsidence trough. Within the mining horizon, the fault was coincident with ground control mitigation features, including a steel canopy in the main roadway and larger, non-uniform pillars in older mine workings. Degraded ground conditions associated with the fault were more pronounced in the eastern portion of the mine. The strike of the fault was approximately parallel with the axis of the Chestnut Ridge anticline and other fault structures described in previous studies (Iannacchione and Coyle 2002).

Jointing observed underground showed multiple orientations, although most joints fell generally into a northwest and northeast set with dips ranging from vertical to less than 30°. One particular set of joints stood out in terms of prominence, persistence, and uniformity. This set, with a strike of N60°W, occurred in a well-defined zone 150 m wide that intersected the main portal area and the eastern half of the pillar collapse zone. Joints in the zone were typically spaced 3–5 m apart and dipped 60–80° to the southwest, as shown in Fig. 4. Some joints traces exposed by the within pillars were curvilinear with dips less than 60° in the lower portion of the pillar. Many of the joints near the collapsed area were dilated by groundwater dissolution and some showed apertures up to 15 cm. The joints, which were perpendicular to both the axis of the Chestnut Ridge anticline and the strike of the thrust fault are interpreted as transverse joints associated with anticline formation.

2.3 Rock Strength and Rock Mass Classification

Rock samples were collected from the operational area of the mine, and five of these samples were tested by the National Institute for Occupational Safety and Health (NIOSH) in accordance with ASTM standard D2398-95 (2002) providing an average uniaxial compressive strength (UCS) of 181.8 MPa, as shown in Table 1. The average UCS is somewhat lower than expected for the Loyalhanna limestone, which is usually in the range of 200–220 MPa (Esterhuizen et al. 2006). However, the lower rock strength is consistent with the rock strength testing results determined during the initial mining permit application to the Pennsylvania Department of Environmental Protection (Smith personal communication 2016).

Rock mass classification of the Loyalhanna limestone at the case study mine was conducted by NIOSH (Esterhuizen et al. 2006) as part of a survey of pillar design practices in limestone mines. The rock mass was classified at three locations using the Bieniawski (1989) rock mass rating (RMR). The unadjusted ratings were found to range from 69 to 76, as shown in Table 2, placing the rock mass slightly below the average RMR of 75 found in the NIOSH survey of US limestone mines (Esterhuizen et al. 2006). The rock mass classification outcome was not used in the assessment of the collapsed pillars, but is provided to allow comparison with other hard rock mines.

2.4 State of Ground Stress

Limestone mines operating within the Loyalhanna limestone can experience roof instability that is related to tectonic horizontal stress within the Mid-North American plate (Iannacchione et al. 2002; Zoback 1992). The limestone beds are much stiffer than the surrounding strata and the pervasive tectonic loading produces greater stress within these stiff beds (Mark and Gadde 2008; Dolinar 2003). At the case study mine, signs of horizontal stress-related roof damage were observed in deeper sections of the mine that are remote from the collapsed area. In the vicinity of the collapsed area, there were no signs of excessive horizontal stress in the roof of the workings. Signs of stress relaxation were rather observed, manifested by the presence of open joints in the roof and in some of the pillars. The absence of the typical high horizontal stress field in this part of the mine is likely the result of the limestone outcropping on three sides around the area of collapsed workings, which provides relief from current day tectonic loading. Stress measurements were not conducted within the limestone beds at the mine.

3 Mining Plan

3.1 Mining Layout and Original Pillar Design

The case study mine employed the room and pillar method which is well suited for extracting flat lying deposits. The method recovers the resource in open stopes or rooms, and pillars are left to support the overlying strata. The rooms and pillars are normally arranged in regular patterns and are equal in size. The aim is to leave the smallest possible pillars to maximize the extraction (Hamrin 2001). When the resource being mined has large vertical height, mining is conducted in horizontal lifts by extracting the floor between the pillars, known as bench mining (Esterhuizen et al. 2007). The room-and-pillar method has the advantage that a minimum of development is needed to recover the resource. Environmental impacts are also minimized because surface subsidence and groundwater disturbances can be minimized in comparison to most other mining methods (Benardos et al. 2001).

The initial mining plan described in the mining permit called for a room-and-pillar layout with 10.7-m × 10.7-m square pillars and rooms that are 13.7 m wide. The limestone bed at the case study mine is up to 20 m thick and therefore mining was planned to be conducted in two lifts, first mining the upper 7.0 m and followed by bench mining between the pillars to increase the mining height to 16.1 m. The layout is thought to be largely driven by mining practices at other mines in the area. The designed pillars, therefore, would have width-to-height ratios of 0.66. The maximum depth of cover under the mountain that

overlies the limestone body is 120 m. In the collapse area, the depth of cover ranges from about 30–90 m.

Figure 5 shows the mining layout and the outline of the area that collapsed. A relatively regular pillar layout was followed starting at the portals, but as the mine progressed, it appears that poor ground conditions were encountered near the low-angle fault exposed in the highwall and underground. As a result, large blocks of ground were left intact with the objective to resume mining beyond the poor ground. During this time, bench mining was conducted in the area near the portals. Bench mining more than doubled the height of the pillars, exposing continuous angular joints that caused sections of the intended pillars to fall away during the blast. Figure 6 shows such a pillar observed around the year 2001 (Iannacchione personal communication 2016).

In subsequent years, portions of the benched area were backfilled with fine crusher waste that may have provided some confinement to the lower half of the pillars. The backfilling did not extend above the mid-height of the benched pillars. The area that collapsed had not been actively mined for approximately 15 years when the collapse occurred. Over the lifetime of the mine, a secondary escapeway had at times passed through the event area.

4   Observations Around the Perimeter of the Collapsed Area

During the inspection mine visit, it was possible to enter the mine through the portal at the northern extent of the mine, right next to the collapsed area. The mine escapeway was open, and it was possible to travel along the northern limit of the collapse and around to the southern extent of the collapse. It appeared that the backfilling material may have prevented some of the benched pillars adjacent to the collapsed area from failing. The exact extent of backfilling was unknown.

4.1   Measured Pillar Dimensions

During an inspection of the collapsed area in August 2016, measurements were made of the actual pillar dimensions around the perimeter of the collapsed area. It was found that the average pillar width was 9.5 m with a standard deviation of 1.3 m. The average room width was 14.5 with a standard deviation of 0.6 m. It was not possible to measure the full height of the pillars within the collapsed area; however, in adjacent stable areas, measurements showed the mining height to be 17.7 m. The average width-to-height ratio is therefore 0.54 with 84% extraction ratio in the room-and-pillar panels.

Figure 7 shows a pillar along the escapeway, which demonstrated the type of roof-to-floor jointing observed in this part of the mine. Note that the walkway was not bench mined and was, therefore, about 10 m above the floor of the benched area.

Figure 8 shows the roof rubble that flowed between the pillars during the collapse. None of the collapsed pillars were visible, owing to the volume of roof rubble that flowed into the mine voids. This raised the question of whether the event may have simply been a roof collapse. However, the significant depth of subsidence, without signs of pillar humps on the surface, and the abruptness of the collapse rules out that the pillars may still be standing in

the collapsed area. A roof collapse would be expected to be more progressive, taking place over an extended period of time.

5   Analysis of Pillar Loading

Back analysis of the pillar strength in a flat-lying collapsed panel is usually based on the assumption that, at the time of collapse, the pillar strength was equal to the imposed overburden load. In this case, the overburden depth varies from about 30 to 90 m, which complicates the calculation of the overburden loading. Also, the overburden load will vary significantly based on the depth. Consequently, the FLAC3D finite difference program (Itasca Consulting Group 2012) was used to create a model of the mountain and the mine workings within the mountain. The model calculated vertical stress within the pillars which was used as an estimate of the actual vertical loading of the pillars.

5.1   Model Setup

The model material was assumed to be elastic so that the pre-failure stress distribution within the collapsed pillars could be determined. The mined-out region was discretized with sufficient detail to simulate the pillars and benched areas. The element width for modeling the mined zone was selected as 2.0 m, allowing each pillar to be modelled with five elements across its width. Pillars were modelled to be 10.0 m wide, and the rooms were modelled to be 14.0 m wide. The overlying strata were modelled using 3-m wide elements. The immediate roof of the mined workings consisted of about 2 m of limestone left intact to prevent breakthrough to the weaker overlying Mauch Chunk strata. This stiffer roof layer was included in the model. Figure 9 shows a cutaway view of the model in which the pillars were horizontally sliced at mid-height and with the mountain shown as a transparent overlay.

The boundary conditions along the sides of the model were set to restrict horizontal displacement only, while the bottom surface was fixed in the vertical direction. The model loading was purely by gravity with horizontal stress only being generated by the Poisson effect of the rock material. As discussed earlier, the presence of outcropping limestone on three sides of the collapsed workings provides relief from horizontal stress associated with current tectonic loading. The model included the "nose" of the mountain, the collapsed workings, and a portion of the mine beyond the collapsed area. The shading of the model shown in Fig. 9 depicts the resulting vertical stress distribution in the pillars and surroundings.

5.2   Pillar Loading Results

The FLAC3D-calculated vertical stress at mid-height of the pillars was used to calculate the average vertical stress in each pillar. The average vertical stress of the individual pillars within the collapsed area varied from the maximum of 11.7 MPa down to 5.3 MPa for the pillars under the shal-lowest cover. A simple tributary area pillar stress calculation, based on a depth of cover of 90 m and 84% extraction, results in an average predicted pillar stress of 13.3 MPa. This slightly higher stress is expected because it assumes a flat ground surface, while the FLAC3D model accurately models the effect of the sloping topography.

The model stress results showed that there was a cluster of five pillars near the edge of the collapsed area, under the ridge of the mountain that had the greatest vertical stress. The calculated average vertical stress in each of these pillars varied from 10.0 to 11.7 MPa, with an average value of 11.0 MPa for the five pillars combined. It was assumed that the collapse initiated when one or more of these pillars failed.

6 Analysis of Pillar Strength

The strength of a pillar in mining applications is usually defined as the peak load bearing capacity of the pillars (Brady and Brown 2006). In the case study mine, the average vertical stress 11.0 MPa in the cluster of five pillars represents the best estimate of the actual strength of the pillars. This pillar strength is only 6% of the intact rock strength as tested in the laboratory. Knowledge of the actual strength of the pillars provides an opportunity to determine whether some of the widely used empirical hard-rock pillar strength equations would have provided reasonable estimates of the pillar strength.

6.1 Comparison of Actual Pillar Strength to Empirical Hard-Rock Pillar Strength Equations

Empirical pillar strength equations are developed from retrospective analysis of actual stable and failed pillar case histories are commonly used to design pillars in mines (Martin and Maybee 2000). Three of the more widely used empirical equations for hard rock mines were selected to calculate the strength of the collapsed pillars at the case study mine. The results were compared to the 11.0 MPa pillar strength determined above. The following three hard rock pillar strength equations were selected for the comparison.The Hedley and Grant (1972) equation:

$$S = k \frac{w^{0.5}}{h^{0.75}} . \tag{1}$$

The Krauland and Soder (1987) equation for limestone pillars:

$$S = k \left(0.778 + 0.222 \left(\frac{w}{h} \right) \right) . \tag{2}$$

The Lunder and Pakalnis (1997) equation:

$$S = 0.44 \sigma_c (0.68 + 0.52 \kappa) . \tag{3}$$

In these equations, k is the large-scale rock strength, w is the pillar width, h is the pillar height, σ_c is the uniaxial compressive strength of the intact rock, and κ is a confinement parameter. The pillar strengths for 17.7-m-high pillars of various widths were calculated using each equation and are shown in Fig. 10. For the Hedley and Grant equation, the strength factor relating the large-scale rock strength to the laboratory-scale UCS is 0.58, and for the Krauland and Soder equation the strength factor is 0.354. The calculated 11.0 MPa pillar strength from this case study is also shown in Fig. 10. It is clear that the empirically

based strength equations would have grossly overestimated the actual pillar strength and would have predicted stable conditions at the mine.

The reason for the discrepancy between the empirical equations and the actual pillar strength at the case study mine is ascribed to the presence of large angular discontinuities cutting through the slender pillars. It appears that the case studies that were used to develop the empirical equations did not include any cases of such slender pillars with large through-going discontinuities. The impact of large through-going discontinuities is also not explicitly included as an input parameter in the selected pillar strength equations.

6.2 Accounting for Large Discontinuities

The potential importance of large through-going discontinuities on the strength of slender pillars was recognized during previous NIOSH research into US limestone mine pillar strength (Esterhuizen et al. 2006; Esterhuizen et al. 2011). Large through-going discontinuities can be defined as planar or semi-planar structures with visible trace lengths greater than 50% of the pillar height. They are typically persistent joints that extend through the pillar or extend from the roof to the floor of a pillar.

During this research, several single pillar failures associated with large through-going discontinuities were observed in otherwise stable workings, but no wide area collapses had occurred that would allow back analysis of average pillar loading and average pillar strength. Simple two-dimensional models of pillars were used, therefore, to investigate the potential impact of large through-going discontinuities on pillar strength. The UDEC (Itasca Consulting Group 2004) discrete element stress analysis software was used to simulate numerous pillar and discontinuity configurations. The model input parameters were selected to correctly simulate the stability of actual pillars with large through-going discontinuities that had not failed.

It was found that the impact of such large through-going discontinuities diminished as the pillar width-to-height ratio increased. Tall, slender pillars were shown to be significantly impacted, while wider pillars at width-to-height ratios exceeding 1.2 showed reduced impact. Discontinuity dips of around 60° were found to have the most significant impact on pillar strength.

Since the established hard-rock pillar strength equations did not explicitly account for the presence of large angular discontinuities, a new design equation for US limestone mines was developed specifically to address this need. The empirical basis for the limestone pillar strength equation was decades of observations of failed and stable pillars by Roberts et al. (2007) in the Missouri lead belt mines. The impact of large discontinuities was introduced as an explicit parameter that accounts for both the frequency and inclination of any large through-going discontinuities, based on the numerical modeling results and field observations. The procedures followed in developing the limestone mine pillar strength equation, together with field data and numerical model results are fully described in Esterhuizen et al. (2011). The equation takes the following form:

$$S = 0.65 \times \text{UCS} \times \text{LDF} \times \frac{w^{0.30}}{h^{0.59}}, \tag{4}$$

where UCS is the uniaxial compressive strength of the intact rock, LDF is a factor to account for the presence of large discontinuities, and w and h are the pillar width and height in meters. The large discontinuity factor accounts for the dip and frequency of the discontinuities as follows:

$$\text{LDF} = 1 - \text{DDF} \times \text{FF}, \tag{5}$$

where DDF is the discontinuity dip factor shown in Table 3 and FF is the frequency factor related to the frequency of large discontinuities per pillar shown in Table 4.

The DDF was developed from the results of numerical model analyses in which single discontinuities at variable dips were modeled in pillars with variable width-to-height ratios. The discontinuities were modeled with 30° friction angle and nominal cohesion of 100–300 kPa to account for joint surface roughness.

The FF accounts for the number of discontinuities within the pillar, again based on numerical model results in which the number and location of discontinuities within pillars of different width-to-height ratios were evaluated. The impact of these discontinuities on the pillar strength was determined from the numerical model results to produce the FF values in Table 4, as described in Esterhuizen et al. (2011).

To simplify the calculation of pillar loads, pillar strength, and the impact of large angular discontinuities, a small software package named S-Pillar (NIOSH 2018) has been developed. The S-Pillar software is now used as a basis for designing pillars in the United States limestone mining industry.

6.3 Application of the Limestone Mine Pillar Strength Equation

The pillar strength equation for limestone mines (Eq. 4) was used to calculate the strength of the collapsed pillars at the case study mine and the results were compared to the 11.0 MPa pillar strength determined above. Based on the available geotechnical data, the following input values and ranges of values were used in the calculation:

> UCS of intact rock = 182 MPa.
>
> Dip of large discontinuities = 50°–80°.
>
> Spacing of large discontinuities = 2–5 m.
>
> Pillar width = 9.5 m.
>
> Pillar height = 17.7 m.

The range of pillar strengths predicted by the equation varied between a minimum of 3.9 MPa for the most unfavorable combination of parameters to 25.3 MPa for the most favorable combination. The range of results obtained is shown in Fig. 11. The indicated range of strengths was determined by varying only the large discontinuity spacing and dip. The

equation predicts minimum strength when the discontinuity dip is 60°. The upper solid curve is obtained by selecting the maximum discontinuity spacing of 5.0 m and a dip of 80°. The figure also shows the pillar strength curve predicted by Eq. (4) in the absence of any large discontinuities.

The results show that Eq. (4) predicts a significant drop in pillar strength at the lower width-to-height ratios. Also, the range of likely strengths based on the variability of the large discontinuity geometry brackets the actual pillar strength of 11.0 MPa. If the average dip and spacing of the most prominent joint set is used as input, at 70° and 4.0 m, respectively, the equation predicts a pillar strength of 12.9 MPa, clearly indicating the potentially critical loading condition of these pillars. By comparison, the Krauland and Soder (1987) pillar strength equation developed for limestone pillars predicts a strength of 57.8 MPa for these pillars, while Eq. (4) predicts a strength of 42.8 MPa in the absence of any large through-going discontinuities.

7 Discussion

The unfortunate events at the case study mine have demonstrated the need to include additional geotechnical parameters in the pillar design equations that are used by the mining industry to design pillars for room and pillar mines. The established pillar strength equations essentially only consider the UCS of the rock and the shape of the pillars, while the discontinuity characteristics and other rock mass-related parameters are excluded. The results of this case study clearly demonstrate the need to explicitly account for the presence of large through-going discontinuities in the estimation of pillar strength. Ignoring these discontinuities using established pillar strength equations would grossly overestimate the pillar strength.

The established empirical pillar strength equations that are widely used for pillar design in room-and-pillar mines do not appear to adequately account for the weakening effect of discontinuities on pillar strength when the width-to-height ratio falls below a value of 1.0. This may be accredited to the limited number of low width-to-height ratio cases included in the empirical databases used for developing the equations. This case study clearly demonstrates how, for example, the Krauland and Soder (1987) empirical pillar strength equation for limestone predicts a strength of 57.8 MPa for the pillars at the case study mine, while they collapsed at a load of only 11.0 MPa.

During the NIOSH survey of limestone mine stability in the United States, numerous single failed pillars that contained through-going discontinuities were observed (Esterhuizen et al. 2006). Analysis of these pillars using established hard-rock pillar strength equations overestimated the strength of these pillars. This led to the realization that such through-going discontinuities needed to be explicitly accounted for in pillar design. The NIOSH-developed pillar strength equation (Eq. 4) made use of field observations and numerical model analysis to develop a relatively simple pillar strength equation that explicitly accounts for the presence of large through-going discontinuities. The NIOSH-developed equation predicts the pillar strength in the collapsed area of the mine as 12.9 MPa when using the 'average' spacing and inclination of the through-going discontinuities, while the lower limit of the

pillar strength is estimated as 3.9 MPa. This result clearly indicates the critical condition of the pillars in question.

The need to incorporate the rock mass strength rather than just the UCS of the rock in pillar design has been recognized by the rock engineering community. Hoek and Brown (1980) suggested combining numerical model analysis with rock mass strength parameters to estimate the strength of pillars. Martin and Maybee (2000) also made use of numerical models to investigate pillar strength in strong rock. More recently, the impact of discrete discontinuities on pillar strength has received increased attention. For example, Elmo and Stead (2010) have used discrete element models to investigate rock mass characteristics and discrete joints on pillar strength, while Oke and Esterhuizen (2017) used a more pragmatic approach to account for both rock mass strength and the impact of discontinuity dip. These approaches are likely to further contribute to improved estimates of pillar strength, especially in the low width-to-height ratio ranges encountered in shallow underground room-and-pillar mines.

8   Conclusions

A case study has been presented in which tall, slender pillars collapsed causing an air blast at a limestone mine in southwestern Pennsylvania. The pillars were about 17 m tall and 9.5 m wide. The collapsed pillars were evaluated using a three-dimensional numerical model to estimate the loading on the pillars. Using these results, it was demonstrated that widely used pillar strength equations for hard-rock mines would have significantly overestimated the strength of the collapsed pillars. It was concluded that large angular discontinuities within the pillars contributed to the collapse. The NIOSH-developed pillar strength equation (Esterhuizen et al. 2011) with an explicit parameter to account for the presence of such through-going discontinuities was shown to be able to satisfactorily capture the reduced strength of the pillars. Pillar design engineers need to be aware of the potential to overestimate the strength of slender pillars that are affected by large angular discontinuities.

Acknowledgements

References

ASTM D2938-95 (2002) Standard test method for unconfined compressive strength of intact rock core specimens. ASTM International, West Conshohocken, CA, 1995

Benardos AG, Kaliampakos DC, Prousiotis JG, Mavrikos AA, Skoparantzos KA (2001) Underground aggregate mining in Athens: a promising investment plan. Tunn Undergr Space Technol 16(4):323–329

Bieniawski ZT (1989) Engineering rock mass classifications. Wiley, New York

Brady BHG, Brown ET (2006) Rock mechanics for underground mining. Springer, Dordrecht

Dolinar D (2003) Variation of horizontal stresses and strains in mines in bedded deposits in the eastern and midwestern United States. In: Proceedings 22nd international conference on ground control in mining, 6–7 August 2003, Morgantown, USA, pp 178–185

Edmunds WE, Berg TM, Sevon WD, Piotrowski RC, Heyman L, Rick-ard RV (1979) The Mississippian and Pennsylvanian (Carboniferous) systems in the United States. USGS professional paper 1110-A-L

Elmo D, Stead D (2010) An integrated numerical modelling discrete fracture network approach applied to the characterization of rock mass strength of naturally fractured pillars. Rock Mech Rock Eng 43:3–19

Esterhuizen GS, Iannacchione AT, Ellenberger JL, Dolinar DR (2006) Pillar stability issues based on a survey of pillar performance in underground limestone mines. In: 25th international conference on ground control in mining, Morgantown, WV, pp 354–361

Esterhuizen GS, Dolinar DR, Ellenberger JL (2007) Observations and evaluation of floor benching effects on pillar stability in US limestone mines. In: 1st Canada–US rock mechanics symposium, American Rock Mechanics Association, Vancouver, BC, Canada, 27–31 May

Esterhuizen GS, Dolinar DR, Ellenberger JL (2011) Pillar strength in underground stone mines in the United States. Int J Rock Mech Min Sci 48(1):42–50

Gillespie P, Kampfer G (2017) Mechanical constraints on kink band and thrust development in the Appalachian plateau, USA, vol 458. Geological Society, London, pp 245–256 (Special Publication)

Hamrin H (2001) Underground mining methods and applications. Underground mining methods: engineering fundamentals and international case studies. In: Hustrulid WA, Bullock RL (eds) Society for Mining, Metallurgy, and Exploration, Inc., Littleton, Colorado, USA, pp 3–14

Hatcher RD, Thomas WA, Viele GW (eds) (1989) The Appalachian-Ouachita Orogen in the United States, vol F-2. Geological Society of America, Boulder, Colorado, p 275

Hedley DGF, Grant F (1972) Stope-and-pillar design for the Elliot Lake uranium mines. Bull Can Inst Min Metall 65:37–44

Hoek E, Brown ET (1980) Underground excavations in rock. England, Institute of Mining and Metallurgy, London, p 200

Iannacchione AT, Coyle PR (2002) An examination of the Loyalhanna limestone's structural features and their impact on mining and ground control practices. In: Peng SS, Mark C, Khair AW, Heasley KA (eds) 21st international conference on ground control in mining, August 6–8, 2002, Morgantown, WV, pp 218–227

Iannacchione AT, Dolinar DR, Mucho TP (2002) High stress mining under shallow overburden in underground U.S. stone mines. In: First international seminar on deep and high stress mining, section 32. Australian Center for Geomechanics, Nedlands, Australia, 11 pp

Itasca Consulting Group (2004) Software: Universal distinct element code (UDEC) version 4.0, Minneapolis, Minnesota

Itasca Consulting Group (2012) Software: Fast Lagrangian analysis of continua in 3 dimensions (FLAC3D) Version 5.01, Minneapolis, Minnesota

Kerrigan R (2016) Structural geology of the southwestern section of the Appalachian Plateau: energy and environments: geology in the 'Nether World' of Indiana County, Pennsylvania. In: Guidebook for the 81st annual field conference of Pennsylvania Geologists, Indiana, Pennsylvania, Editors: Anthony Robin, pp 3–10

Krauland N, Soder PE (1987) Determining pillar strength from pillar failure observations. Eng Min J 8:34–40

Lunder PJ, Pakalnis R (1997) Determination of the strength of hard-rock mine pillars. Bull Can Inst Min Metall 90:51–55

Mark C, Gadde M (2008) Global trends in coal mine horizontal stress measurements. In: Proceedings 27th international conference on ground control in mining, WV University, Morgantown, USA, pp 319–331

Martin CD, Maybee WG (2000) The strength of hard-rock pillars. Int J Rock Mech Min Sci 37(8):1239–1246

Mount VS (2014) Structural style of the Appalachian Plateau fold belt, north-central Pennsylvania. J Struct Geol 69:284–303

Nickelsen RP, Hough VND (1967) Jointing in the Appalachian plateau of Pennsylvania. Geol Soc Am Bull 78(5):609–630

NIOSH (2018) Mining product: S-pillar—software for stone mine pillar design. National Institute for Occupational Safety and Health. https://www.cdc.gov/niosh/mining/works/coversheet1817.html. Accessed 16 Oct 2018

Oke J, Esterhuizen GS (2017) Improving hard rock pillar design by including rock mass classification and failure mechanisms. In: 51st US rock mechanics/geomechanics symposium, San Francisco, California, 25–28 June

Roberts D, Tolfree D, McIntyre H (2007) Using confinement as a means to estimate pillar strength in a room and pillar mine. In: 1st Canada–US rock mechanics symposium, American Rock Mechanics Association, Vancouver, BC, Canada, 27–31 May, pp 1455–1461

Rodgers J (1970) The tectonics of the Appalachians. Wiley, New York

Sak PB, McQuarrie N, Oliver BP, Lavdovsky N, Jackson MS (2012) Unraveling the central Appalachian fold-thrust belt, Pennsylvania: the power of sequentially restored balanced cross section for a blind fold–thrust belt. Geosphere 8(3):685–702

Trapp H Jr, Horn MA (1997) Ground water atlas of the United States—delaware, Maryland, New Jersey, North Carolina, Pennsylvania, Virginia, West Virginia. USGS Hydrologic Atlas 730–L

Zoback ML (1992) First- and second-order patterns of stress in the lithosphere: the world stress map project. J Geophys Res 97(11):703–711

Fig. 1.
Aerial view of the mine showing extent of surface subsidence associated with the collapse of the pillars
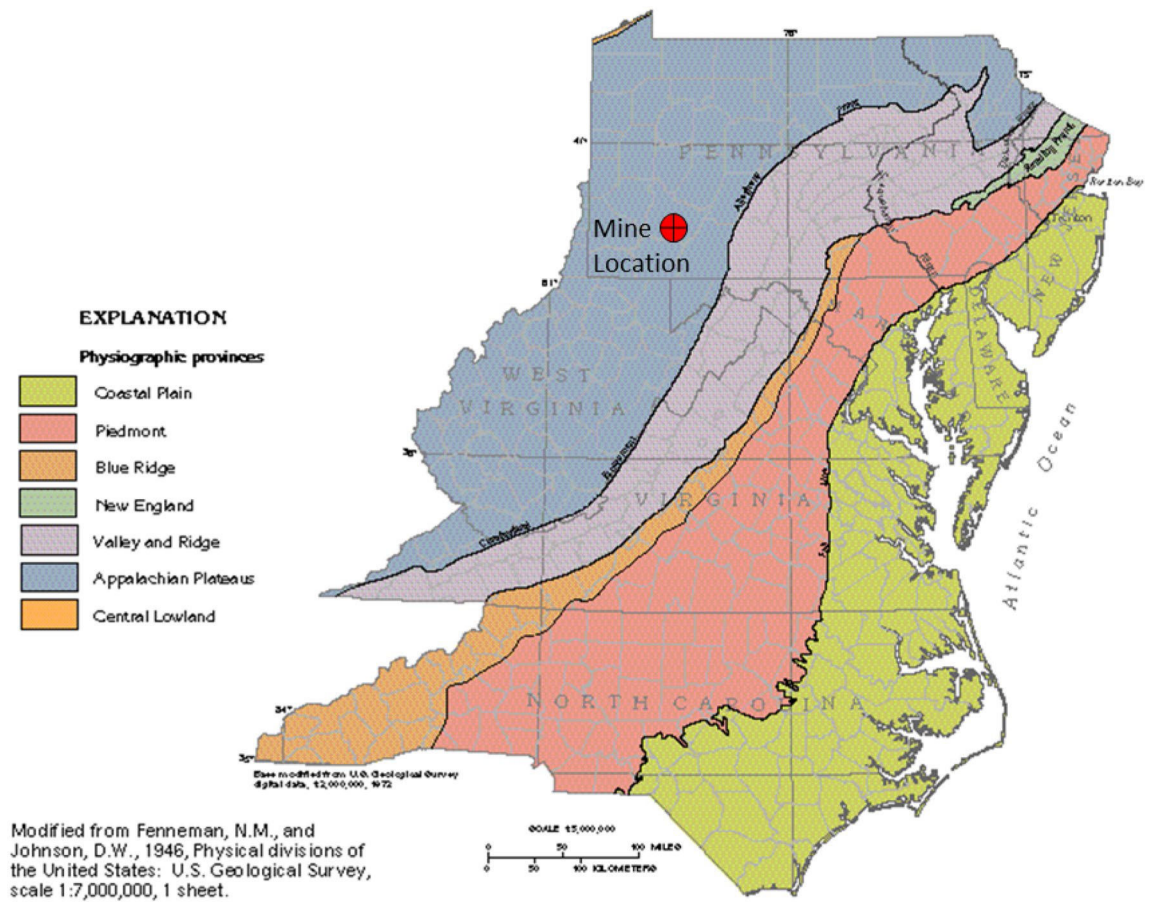
EXPLANATION

Physiographic provinces

- Coastal Plain
- Piedmont
- Blue Ridge
- New England
- Valley and Ridge
- Appalachian Plateaus
- Central Lowland

Modified from Fenneman, N.M., and Johnson, D.W., 1946, Physical divisions of the United States: U.S. Geological Survey, scale 1:7,000,000, 1 sheet.

Fig. 2.
Mine location and physiographic provinces of the Appalachian Mountains

Fig. 3.
Access portal entering the mine with Mauch Chunk beds exposed in the highwall

Fig. 4.
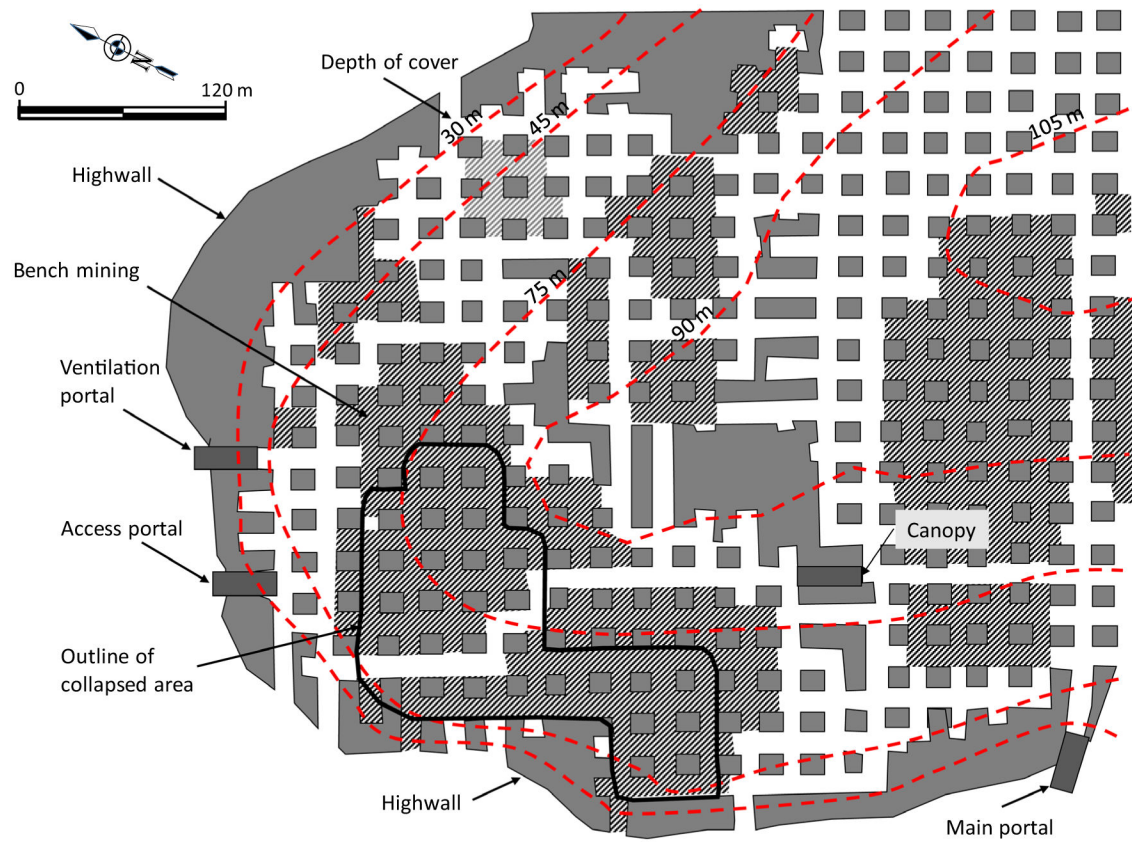Prominent N60°W striking joint intersecting a pillar south of the collapsed area

Fig. 5.
Plan view of the mine workings showing the room-and-pillar layout, the outline of the collapsed area and depth of cover contours

Fig. 6.
Pillar impacted by large angular joints along the edge of bench mining showing sections of the pillar that fell away during bench mining (photo by A. T. Iannacchione)

Fig. 7.
Pillar affected by angular jointing adjacent to the collapsed area

Fig. 8.
Rubble from the roof collapse and a stable pillar along the edge of the area that collapsed
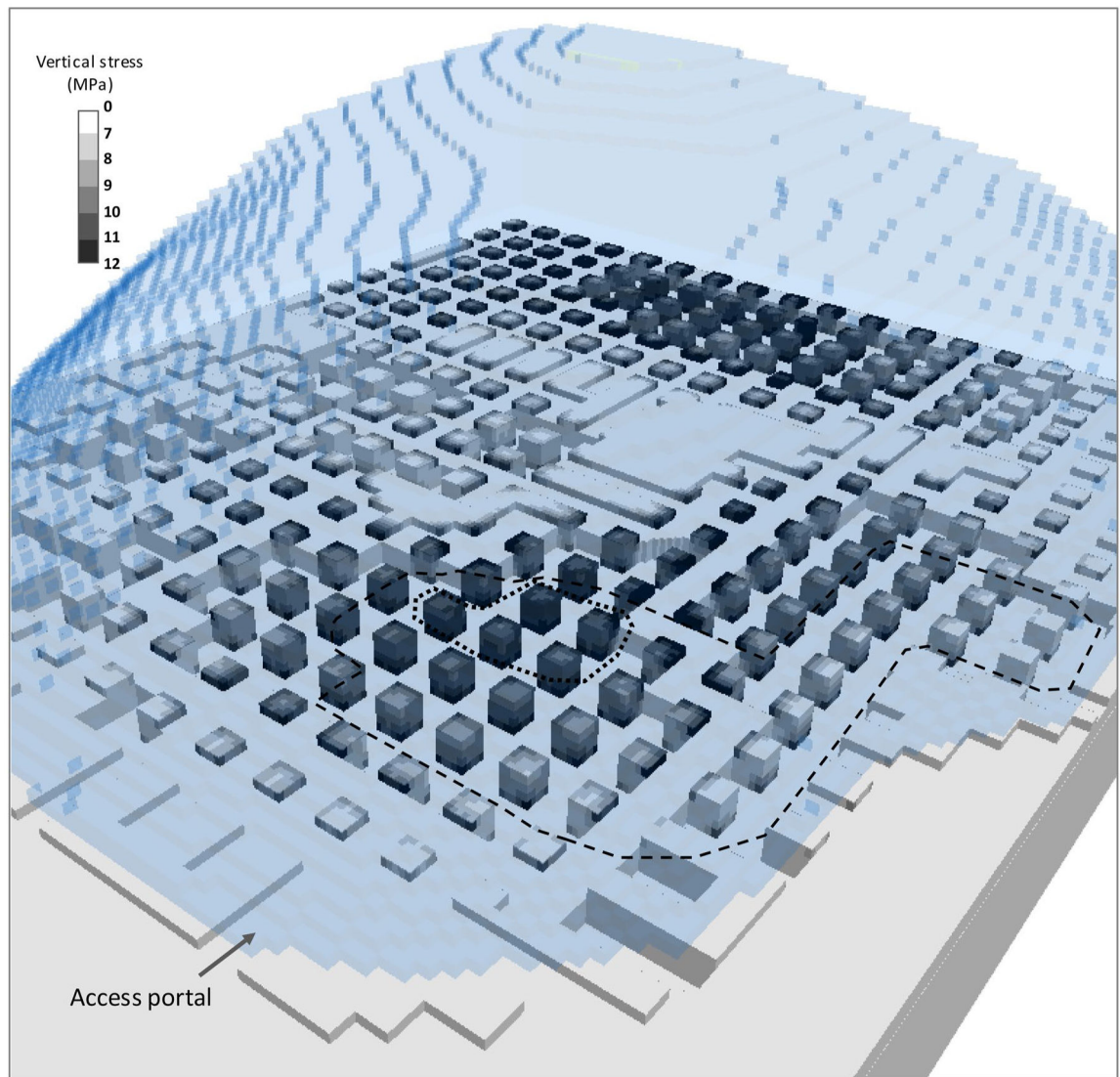
Fig. 9.
Numerical model of the mine and overlying mountain shaded by the vertical stress magnitude. The collapsed area is outlined with dashed lines, and the cluster of pillars with the highest average vertical stress is outlined with a dotted line
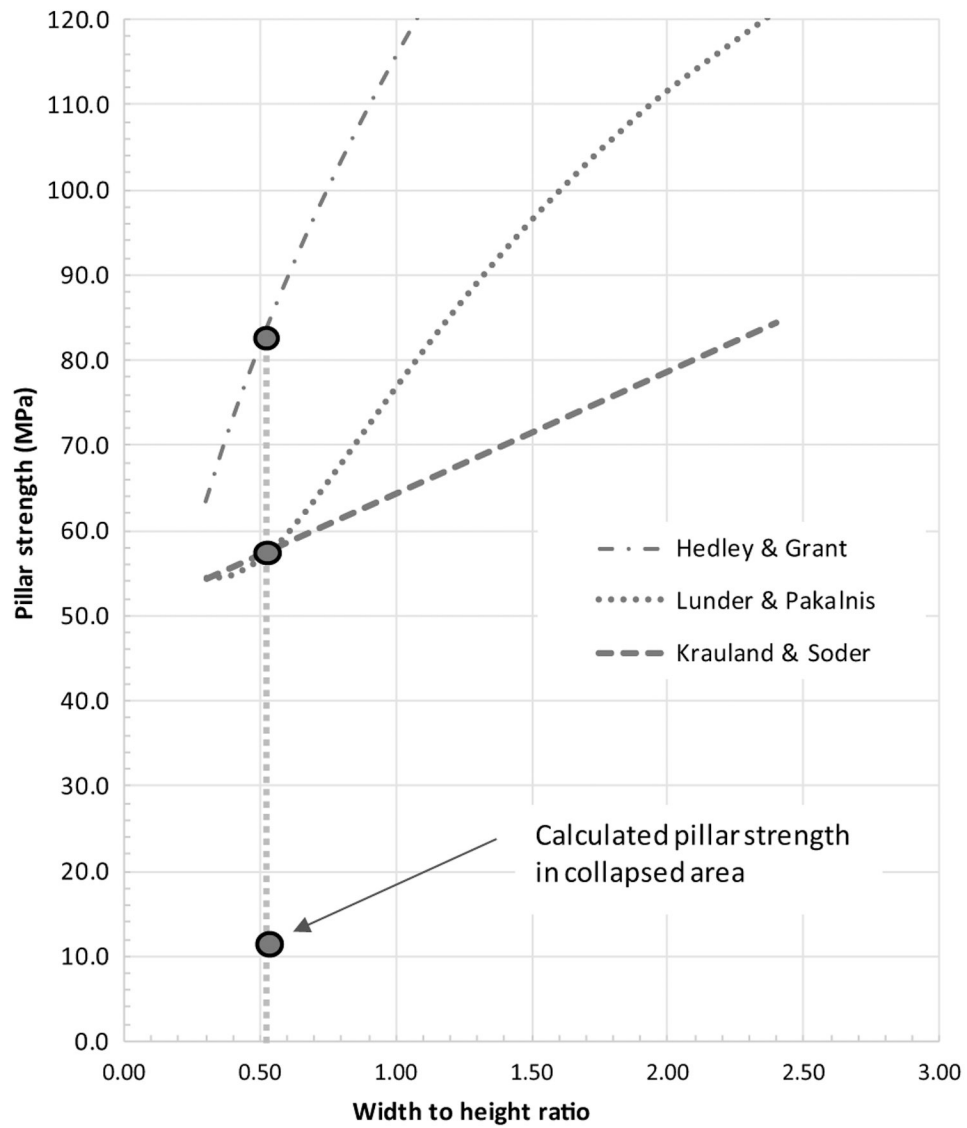
Fig. 10.
Calculated pillar strength in the collapsed area compared to predictions using established hard-rock pillar strength equations
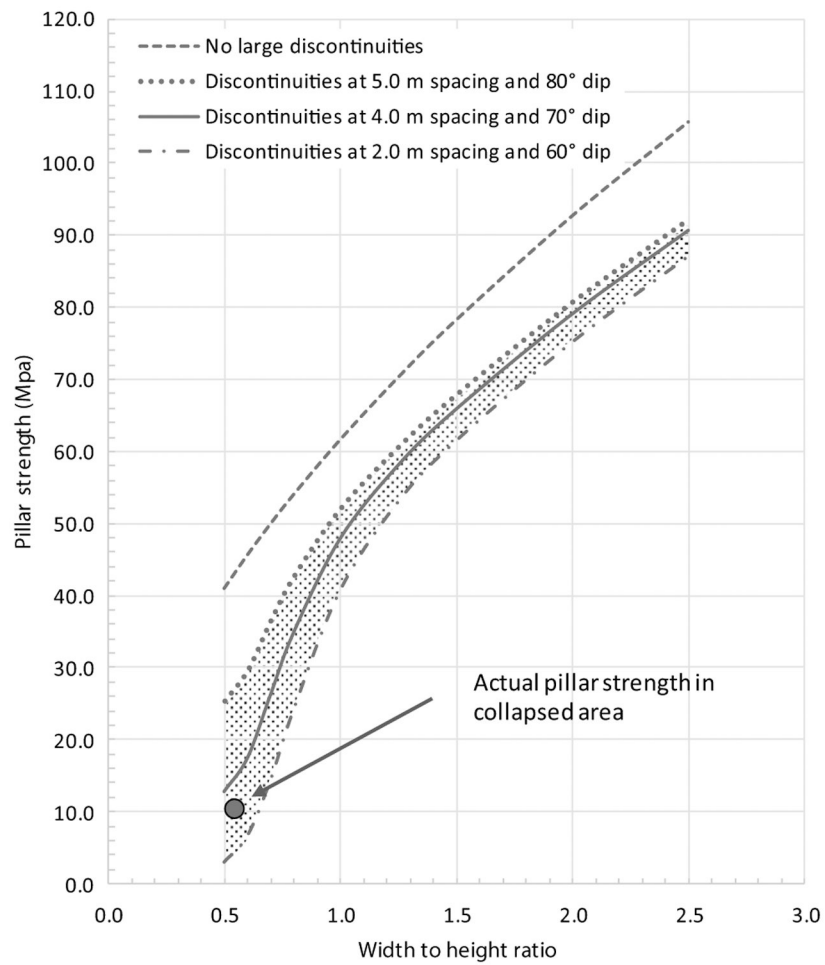
Fig. 11.
Graph showing the likely range of pillar strengths for different width-to-height ratios at the
case study mine calculated using Eq. (4). The range of likely pillar strengths is shaded and
the actual strength of 11.0 MPa of the collapsed pillars is indicated on the graph

Table 1

Uniaxial compressive strength (UCS) testing results of core samples collected from the case study mine

Sample no.	UCS (MPa)	Tangent elastic modulus at 50% of peak strength (GPa)	Poisson's ratio at 50% of peak strength	Specific gravity
1	173.6	38.4	0.17	2.70
2	174.4	46.1	0.17	2.75
3	182.5	46.6	0.04	2.63
4	186.4	47.2	0.20	2.66
5	192.1	51.9	0.18	2.68
Average	181.8	46.1	0.20	2.70

Table 2

Rock mass classification conducted at three sites in the case study mine using the Bieniawski (1989) rock mass rating (RMR89)

Site no.	Rock strength rating	RQD rating	Joint Spacing rating	Joint condition rating	Ground water rating	RMR89
1	12	12	11	24	15	74
2	12	12	10	27	15	76
3	12	8	8	26	15	69
Average	12.0	10.7	9.7	25.7	15.0	73

Table 3

The discontinuity dip factor (DDF) representing the strength reduction caused by a single discontinuity intersecting a pillar at or near its center, used in Eq. (5) (Esterhuizen et al. 2011)

Dip (°)	Pillar width-to-height ratio								
	0.5	0.6	0.7	0.8	0.9	1.0	1.1	1.2	> 1.2
30	0.15	0.15	0.15	0.15	0.16	0.16	0.16	0.16	0.16
40	0.23	0.26	0.27	0.27	0.25	0.24	0.23	0.23	0.22
50	0.61	0.65	0.61	0.53	0.44	0.37	0.33	0.30	0.28
60	0.94	0.86	0.72	0.56	0.43	0.34	0.29	0.26	0.24
70	0.83	0.68	0.52	0.39	0.30	0.24	0.21	0.20	0.18
80	0.53	0.41	0.31	0.25	0.20	0.18	0.17	0.16	0.16
90	0.31	0.25	0.21	0.18	0.17	0.16	0.16	0.15	0.15

Table 4

The frequency factor (FF) used in Eq. (5) to account for the spacing of large discontinuities (Esterhuizen et al. 2011)

Average frequency of large discontinuities per pillar	Frequency factor (FF)
0.0	0.00
0.1	0.10
0.2	0.18
0.3	0.26
0.5	0.39
1.0	0.63
2.0	0.86
3.0	0.95
> 3.0	1.00